Higher sensitivity towards light stress and ocean acidification in an Arctic sea-ice-associated diatom compared to a pelagic diatom

Ane C. Kvernvik[1],* (iD), Sebastian D. Rokitta[2]* (iD), Eva Leu[3] (iD), Lars Harms[2] (iD), Tove M. Gabrielsen[1,4] (iD), Björn Rost[2,5] (iD) and Clara J. M. Hoppe[2] (iD)

[1]The Department of Arctic Biology, Svalbard Science Centre, University Centre in Svalbard, PO Box 156, N-9171, Longyearbyen, Norway; [2]Marine Biogeosciences, Alfred-Wegener-Institut – Helmholtz-Zentrum für Polar- und Meeresforschung, Am Handelshafen 12, 27570 Bremerhaven, Germany; [3]Arctic R&D, Akvaplan-Niva AS, CIENS, Gaustadalleen 21, 0349 Oslo, Norway; [4]Faculty of Engineering and Science, University of Agder, PO Box 422, N-4604, Kristiansand, Norway; [5]FB2, University of Bremen, Leobener Strasse, 28359 Bremen, Germany

Summary

- *Thalassiosira hyalina* and *Nitzschia frigida* are important members of Arctic pelagic and sympagic (sea-ice-associated) diatom communities. We investigated the effects of light stress (shift from 20 to 380 μmol photons m^{-2} s^{-1}, resembling upwelling or ice break-up) under contemporary and future pCO_2 (400 vs 1000 μatm).
- The responses in growth, elemental composition, pigmentation and photophysiology were followed over 120 h and are discussed together with underlying gene expression patterns.
- Stress response and subsequent re-acclimation were efficiently facilitated by *T. hyalina*, which showed only moderate changes in photophysiology and elemental composition, and thrived under high light after 120 h. In *N. frigida*, photochemical damage and oxidative stress appeared to outweigh cellular defenses, causing dysfunctional photophysiology and reduced growth. pCO_2 alone did not specifically influence gene expression, but amplified the transcriptomic reactions to light stress, indicating that pCO_2 affects metabolic equilibria rather than sensitive genes.
- Large differences in acclimation capacities towards high light and high pCO_2 between *T. hyalina* and *N. frigida* indicate species-specific mechanisms in coping with the two stressors, which may reflect their respective ecological niches. This could potentially alter the balance between sympagic and pelagic primary production in a future Arctic.

Introduction

The Arctic Ocean is changing in many respects, with declining sea ice cover and increasing pCO_2 being among the most rapidly changing factors (IPCC, 2014). Irradiance levels in the upper mixed layer are expected to increase due to increased thermal stratification, declining snow cover, earlier melt onset accompanied by formation of melt ponds, and reduced summer sea-ice extent (Screen & Simmonds, 2010; Nicolaus *et al.*, 2012; Tremblay *et al.*, 2015). In addition, ocean acidification (OA) is most pronounced in the Arctic because CO_2 solubility increases at low temperatures, and the low total alkalinity makes the system sensitive to anthropogenic CO_2 loading (Yamamoto-Kawai *et al.*, 2009; AMAP, 2018). These two factors, namely irradiance regimes and pCO_2 levels, may not only affect the physiological performance, but also competitiveness and nutritional value of microalgae (Rost *et al.*, 2008; Kroeker *et al.*, 2013; Gao & Campbell, 2014; McMinn, 2017).

To cope with instantaneous high light stress, diatoms utilize diverse mechanisms involving short- and long-term physiological changes. Short-term changes involve increased nonphotochemical quenching (NPQ) of excitation energy, facilitated by the de- and re-epoxidation of the xanthophylls diadinoxanthin (DD) and diatoxanthin (DT). These pigments thermally dissipate excess excitation energy (Lavaud & Goss, 2014) and decrease overall stress derived from electron pressure and reactive oxygen species. Over longer time scales, diatoms alter pigment composition, typically increasing pigments related to photoprotection while decreasing those related to light harvesting (Brunet *et al.*, 2011). Studies have shown, however, that responses to changing light intensities can be modulated by high pCO_2 (Rost *et al.*, 2006; Li & Campbell, 2013; Hoppe *et al.*, 2015), which is often attributed to carbon concentrating mechanisms (CCMs) that elevate CO_2 concentrations around Rubisco under current, potentially limiting conditions (Giordano *et al.*, 2005). The expected increase in oceanic pCO_2 may cause a downregulation in the CCM activity of diatoms due to increased diffusive CO_2 uptake,

or decreased leakage as a result of a smaller outward CO_2 gradient (Trimborn *et al.*, 2009). Because CCMs are energetically expensive (Hopkinson *et al.*, 2011; Raven *et al.*, 2014), this may allow for optimization of their energy allocation potentially increasing carbon fixation (Van der Waal *et al.*, 2019). Other studies indicate that the sensitivity of diatoms to high light stress increases under OA (Gao *et al.*, 2012; Hoppe *et al.*, 2015). These findings emphasize large inter- and intraspecific differences in CO_2 sensitivities, but also the potential for the interactive nature of CO_2 and light effects (Rost *et al.*, 2008; McCarthy *et al.*, 2012; Wolf *et al.*, 2018). Hence, major alterations in bloom timing and the composition of algal assemblages can be expected as a result of ongoing environmental changes. One of the major open questions remains, however, whether potential differences in phenotypic plasticity of species may lead to shifts in the relative importance of primary production derived from pelagic vs sympagic (sea-ice-associated) algae in the future Arctic ocean.

Both the pelagic and the sympagic ecosystems host diverse and distinct microalgal communities, which exhibit specific adaptations to their respective habitats with contrasting physico-chemical qualities (Poulin *et al.*, 2011). Arctic pelagic communities are typically exposed to strong and rapid fluctuations in light regimes due to wind-driven overturning (MacIntyre *et al.*, 2000) and attenuation by sediment loading from riverine as well as glacial runoff (Hasholt *et al.*, 2006). Yet, the regimes of temperature, salinity and carbonate chemistry are comparably stable. Hence, we hypothesized that pelagic algae are highly resilient towards photophysiological stress, while being responsive to OA. Within sea-ice, light intensities are extremely low, and fluctuations therein are small and typically change slowly as snow and ice melt (Hill *et al.*, 2018). However, sympagic ice-algal communities need to tolerate subzero temperatures, sustain net growth under such low irradiances (Hancke *et al.*, 2018), and tolerate high salinities and extremely variable nutrient levels as well as distorted carbonate chemistry (Weeks & Ackley, 1986; McMinn *et al.*, 2014; Hill *et al.*, 2018). Despite the extreme physico-chemical properties of this habitat, ice-algae are widespread and often thrive remarkably well as both their productivity and biomass can reach very high levels in spring (Aletsee & Jahnke, 1992; Gradinger, 2009). Hence, we hypothesized that ice-algae can cope less well with instantaneous light stress, but exhibit high physiological plasticity to changing pH/CO_2 regimes under OA.

To investigate the responses of pelagic and sympagic diatoms, the common species *Thalassiosira hyalina* (Hegseth & Sundfjord, 2008) and *Nitzschia frigida* (Syvertsen, 1991; Leu *et al.*, 2015) were acclimated to low light (20 µmol photons m^{-2} s^{-1}) and then exposed to a high light scenario (380 µmol photons m^{-2} s^{-1}) that resembled upwelling, ice break-up or melt-pond formation (Light *et al.*, 2015; Alou-Font *et al.*, 2016). This was done under contemporary and future pCO$_2$ (400 vs 1000 µatm), so that the effects of high light and OA can be investigated in isolation and combination. We followed the phenomenological and physiological reactions over a time course of several days and assessed the accompanying gene expression patterns to explore the underlying mechanisms that determine these species' performances in a changing Arctic.

Materials and Methods

Culture conditions and experimental set-up

Dilute batch cultures of *T. hyalina* (Grunow) Gran 1897 and *N. frigida* Grunow 1880 were grown in 1 liter borosilicate bottles in 0.2 µm sterile-filtered Arctic seawater enriched with trace metals and vitamins according to f/2 media (Guillard & Ryther, 1962). Nitrate, phosphate and silicate were added in concentrations of 100, 25 and 60 µmol l^{-1}, respectively. *Thalassiosira hyalina* cultures were diluted every 2–4 d (yielding 500–6000 cells ml^{-1}), while *N. frigida* was diluted every 3–5 d (yielding 1000–10 000 cells ml^{-1}) to minimize cellular shading, nutrient limitation and biomass-dependent changes in carbonate chemistry. Cells were grown under constant low light (LL; *c.* 20 µmol photons m^{-2} s^{-1}), provided by daylight lamps (Biolux T8, 6500K; Osram, München, Germany) and at two different CO_2 partial pressures (pCO$_2$; 400 vs 1000 µatm). Cultures were acclimated to these conditions for > 8 generations, before cells were exposed to high light (HL; *c.* 380 µmol photons m^{-2} s^{-1}). Irradiance was measured in cell-free culture bottles using a ULM-500 data logger (Li-Cor, Lincoln, NE, USA) equipped with a 4π sensor (Walz, Effeltrich, Germany). Bottles were placed in well-mixed aquaria with continuous temperature surveillance (Almemo 2890; Ahlborn, Holzkirchen, Germany) to ensure temperature stability (2.3 ± 0.3 and 2.8 ± 0.4°C for LL and HL, respectively). After the cells were exposed to HL, the immediate and the acclimation responses (after 5–7 d) were measured for each species. Growth rates, particulate organic carbon and nitrogen (POC and PON) quotas as well as pigment composition were determined in four biological replicates per treatment, with the exception of *N. frigida* in HL, where three replicates were taken. Fluorescence-based photosynthesis measurements were conducted in biological triplicates.

Carbonate chemistry

Target pCO$_2$ was established by aerating the bottles with humidified air containing 400 and 1000 µatm CO_2, respectively, delivered through 0.2 µm sterile filters (Midisart 2000; Sartorius Stedim, Göttingen, Germany). Gas mixtures were generated by a gas mixing system as described by Hoppe *et al.* (2015). The stability of carbonate chemistry was ensured by daily pH measurements (NBS scale; Aquatrode plus Pt1000; Metrohm, Herisau, Switzerland). Samples of total alkalinity (TA) and dissolved inorganic carbon (DIC) were taken from each replicate as well as cell-free control bottles. TA samples were filtered (GF/F; Whatman, Maidstone, UK) and stored at *c.* 4°C until analysis. TA was measured by titration (Dickson, 1981) using a TitroLine burette (Schott Instruments, Mainz, Germany). DIC samples were filtered (0.2 µm cellulose-acetate syringe filters; Sartorius Stedim Biotech) and stored head-space free in 5 ml gas-tight borosilicate bottles at *c.* 4°C. DIC was determined using a QuaAAtro autoanalyzer (Seal Analytical, Norderstedt, Germany) following the method of Stoll *et al.* (2001). The carbonate system was calculated from DIC, pH, salinity, temperature, phosphate and silicate using the CO$_2$Sys program (Pierrot *et al.*, 2006; Table 1).

Growth, size and production rates

Cell concentrations were determined daily using a Multisizer III (Beckman-Coulter, Brea, CA, USA). To disrupt *N. frigida* chains, the cultures were shaken at 1500 rpm for 15 s (Precellys Evolution; Bertin, Bretinneux, France). Microscopy (Axio Observer.D1; Zeiss, Oberkochen, Germany) showed only single, intact cells after shaking. Specific growth rates (μ) were calculated by exponentially fitting the cell numbers over several days. Size was determined via light microscopy and Coulter Counter. For POC and PON quotas, cells were filtered onto precombusted (15 h, 500°C) glass fiber filters (GF/F; Whatman) and stored at $-20°C$ until further processing. Filters were soaked with 200 μl 0.2 mol l^{-1} HCl to remove residual inorganic carbon before measurements (EuroVector EA, EuroVector, Milan, Italy). POC production rates were calculated by multiplying the POC quota with the specific growth rate of the respective incubation.

Pigment composition

Samples were collected on GF/F filters (Whatman), flash-frozen in liquid nitrogen and stored at $-80°C$ until analysis. Filters were extracted for 24 h in a Teflon-lined tube with 1.6 ml 95% methanol, and then refiltered through 0.45 μm filters (Millipore, Billerica, MA, USA), before the final extract was submitted to HPLC analysis. Pigment analyses followed Rodriguez *et al.* (2006) using an HP1100 HPLC system (Hewlett-Packard, Ramsey, MN, USA). The identification of pigments was based on retention times, pigment spectra obtained with a diode array OD detector and commercially available pigment standards (Rodriguez *et al.*, 2006).

Chl*a* variable fluorescence

Chl *a* variable fluorescence was measured using a Fast Ocean FRR fluorometer combined with a FastAct system (Chelsea Technologies, West Molesey, UK). Constant water pumping from the aquaria through the FastAct chamber prevented thermal change during measurements. Samples of *T. hyalina* and *N. frigida* were dark-acclimated inside the FastAct for 10 min before being exposed to a weak measuring light to record initial fluorescence (F_0). Saturation flashlets (blue LED color; 450 nm) were applied to saturate photosystem II (PSII) in order to determine maximal fluorescence (F_m) and the absorption cross section of PSII (σ_{PSII}; nm^2 $PSII^{-1}$), followed by a sequence of relaxation flashlets (Oxborough *et al.*, 2012). Details on assay settings are given in Supporting Information Table S1. To record photosynthesis vs irradiance (PE) curves, the FastAct provided 10×3 min levels of white photosynthetically active radiation ranging from 0 to 1507 μmol photons m^{-2} s^{-1}. Following these actinic light periods, minimum (F_0') and maximum (F_m') fluorescence in light-acclimated cells was determined and electron transfer rates through PSII $cell^{-1}$ (ETR (fmol e^- per cell h^{-1})) were calculated as (Hughes *et al.*, 2018):

$$\text{ETR} = E \cdot \frac{F_m \cdot F_o'}{F_m - F_o} \cdot \frac{K_a}{1000000} \cdot F_q'/F_m'.$$

From the generated PE curves, the light utilization coefficient (α (fmol e^- per cell h^{-1} (μmol photons m^{-2} $s^1)^{-1}$) and the maximum photosynthetic rate (ETR$_{max}$ (fmol e^- per cell s^{-1})) were derived by nonlinear regression using the model of Eilers & Peeters (1988). The light acclimation index E_k was then calculated as ETR$_{max}$/α. The quantum yield of regulated (Y(NPQ)) and nonregulated NPQ (Y(NO)) of Chl*a* fluorescence was calculated at 1000 μmol photons m^{-2} s^{-1} according to Klughammer & Schreiber (2008):

$$\text{Y(NPQ)} = \frac{F'}{F_m'} - \frac{F'}{F_m}$$

$$Y(\text{NO}) = \frac{F'}{F_m}$$

Table 1 Seawater carbonate chemistry at the end of low light (LL) and high light (HL) treatments ($n = 4$; mean $\pm$ 1 SD).

Species	Light	Target pCO$_2$ (μatm)	Measured analytically			Calculated with CO$_2$Sys	
			pH total scale	TA (μmol kg^{-1})	DIC (μmol kg^{-1})	Dissolved CO$_2$ (μmol kg^{-1})	pCO$_2$ (μatm)
T. hyalina	LL	400	8.09 ± 0.01	2540 ± 11	2327 ± 12	21.7 ± 0.2	384 ± 3
T. hyalina	HL	400	8.15 ± 0.05	2529 ± 81	2236 ± 71	17.9 ± 2.5	316 ± 44
Control		400	8.09	2493	2268	20.9	362
T. hyalina	LL	1000	7.71 ± 0.01	2518 ± 33	2388 ± 25	53.9 ± 1.0	952 ± 18
T. hyalina	HL	1000	7.77 ± 0.05	2558 ± 14	2330 ± 32	45.7 ± 5.5	807 ± 98
Control		1000	7.74	2510	2360	49.71	857
N. frigida	LL	400	8.09 ± 0.01	2794 ± 30	2449 ± 18	22.9 ± 0.7	405 ± 12
N. frigida	HL	400	8.10 ± 0.01*	2759 ± 50*	2456 ± 11*	22.3 ± 0.5*	393 ± 8*
Control		400	8.07	2593	2477	23.8	413
N. frigida	LL	1000	7.68 ± 0.03*	2846 ± 9*	2513 ± 9*	61.6 ± 3.4*	1088 ± 60*
N. frigida	HL	1000	7.73 ± 0.01	2771 ± 66	2483 ± 13	53.9 ± 1.1	951 ± 20
Control		1000	7.71	2723	2507	56.1	967

The carbonate system was calculated from dissolved inorganic carbon (DIC), pH, salinity (32.7), temperature (3°C), phosphate (6.3 μmol kg^{-1}) and silicate (100 kg^{-1}) using the CO$_2$Sys program (Pierrot *et al.*, 2006). In addition, samples of total alkalinity (TA) were taken from each replicate. Four control bottles that contained sterile medium were aerated with pCO$_2$ of 400 and 1000 μatm and sampled at the same time as *Thalassiosira hyalina* and *Nitzschia frigida*. *, $n = 3$; mean $\pm$ 1 SD.

Statistical analysis

All data presented are means of three or four replicates ± SD. To test whether HL exposure significantly affected algal photophysiology (F_v/F_m, σ_{PSII}, Y(NPQ), Y(NO), α, ETR and E_k) or pigment quotas at different time points, one-way repeated measures (RM) ANOVA with subsequent normal distribution (Shapiro–Wilk) and *post-hoc* tests (Bonferroni *t*-test) were performed (Table S2). Two-way ANOVA with *post-hoc* tests (Holm–Sidak) were used to evaluate responses in POC and PON quotas, POC production, size fractions and growth rates (Table S3), as well as the responses to high and low pCO$_2$ in LL- and HL-acclimated cells (Table S4). Statistical analyses were performed using the program SIGMAPLOT (SysStat Software, San Jose, CA, USA). Responses were deemed significant at $P \leq 0.05$.

Differential gene expression analyses

A detailed description of the materials and methods used in the differential gene expression (DGE) analyses can be taken from Methods S1 and Notes S1. In brief, 1 µg of RNA was used to prepare a cDNA library (TruSeq HT paired end kit, Illumina, San Diego, CA, USA) that was sequenced in a High Output FlowCell V2 (Illumina) using a NextSeq 500 sequencer (Illumina). Trimmed raw data are accessible at www.ebi.ac.uk under accession no. E-MTAB-6999. Quality checks (FASTQC; Andrew, 2010; Table S5) showed that < 7% of the runs yielded low read numbers. Because replication was sufficiently high, these samples could be excluded from further analyses without disabling statistical evaluation (Table S5). Sequences of adapters and the Illumina spike-in 'PhiX' as well as remaining rRNA sequences were removed (BBTOOLS; Bushnell, 2015; SORTMERNA; Kopylova *et al.*, 2012) before a final quality trimming was performed (BBTOOLS; Bushnell, 2015). Sequences were then normalized (Bushnell, 2015) and *de novo* assembled (TRINITY; Grabherr *et al.*, 2011), yielding 43 554 or 52 411 putative transcripts for *T. hyalina* and *N. frigida*, respectively (Table S6; https://doi.org/10.5281/zenodo.3361258, BLASTX annotation; Table S8).

Genomics Workbench 10 (CLC Biosciences, Aarhus, Denmark) was used for DGE analyses. Reads were mapped to the transcripts, and read counts were tested for statistically significant regulation patterns. Lastly, the significance estimates of DGE patterns were corrected for the statistical false discovery rate (FDR; Benjamini & Hochberg, 1995). To visualize and better compare expression patterns further, total read counts were normalized to intrasample sequencing depth, yielding the reads per kilobase per million mapped nucleotides (RPKM; Mortazavi *et al.*, 2008). To account for different sequencing depths between samples, a TMM-Normalization (Robinson & Oshlack, 2010) was implemented. To isolate DGE patterns and yield a manageable size, the complete expression datasets (https://doi.org/10.5281/zenodo.3523305) of 43 554 or 52 411 transcripts of *T. hyalina* and *N. frigida* were reduced. To this end, we subtracted irrelevant transcripts to retain only those transcripts that were significantly regulated and of interest. Specifically, we retained transcripts that exhibited significant regulation (FDR-corrected $P \leq 0.05$) and an average RPKM-based fold-change value ≥ 2.5 between the initial (0 h) and the first time point (2 h) in any of the pCO$_2$ levels. In addition, we retained transcripts that had an average RPKM-based fold-change value of ≥ 2.5 between 2 and 24 h in any of the pCO$_2$ levels, because re-acclimation occurred between these time points. Lastly, transcripts were retained that were highly expressed throughout the datasets, that is having mean RPKM expression levels ≥ 150 across both pCO$_2$ levels. These retained transcripts (9084 and 9976 for *T. hyalina* and *N. frigida*, respectively) were then annotated using BLASTX (Altschul *et al.*, 1990) and the NCBI RefSeq database (October 2017). The two best hits for every transcript were concatenated to the expression data, yielding DGE datasets of 5954 and 6143 transcripts of interest including their best- and second-best annotation (Table S7).

To assess possible OA modulation of the observed HL responses, datasets were first examined towards transcripts that experienced a synonymous unidirectional regulation in both pCO$_2$ levels (i.e. transcripts that experienced either a HL-dependent up- or downregulation throughout the time course). For those transcripts that reacted synonymously to the HL treatment, the pCO$_2$-related intensity change of the HL response in every time step was calculated by dividing the respective fold-changes from the time course.

Results

Results of the HL exposure time course are reported separately for *T. hyalina* and *N. frigida* by comparing parameters between different time-points in cells grown at 400 µatm. After that, the effect of pCO$_2$ on the HL response in both species is described. Regarding DGE, the obtained reduced datasets were subjected to a clustering approach using Euclidean distances (Fig. S1). Clustering showed that besides having transcripts that were not differentially patterned, the dataset contained mostly transcripts that experienced a coherent down- or upregulation followed by a reversion to near-baseline expression in both pCO$_2$ levels. Expression data with statistical significance tests, as well as functional classification of genes, are presented in Table S7.

HL responses in *T. hyalina*

During the first 12 h of HL exposure, the maximum dark-acclimated PSII quantum yield (F_v/F_m; Fig. 1a; Table S2) decreased in *T. hyalina* from initially 0.60 ± 0.01 under LL to 0.32 ± 0.02. Thereafter, F_v/F_m increased again and, after 72 h, stabilized at a significantly lower level compared to LL (0.41 ± 0.03). The absorption cross-section of PSII (σ_{PSII}) increased rapidly during the first 15 min of HL exposure (from 3.4 ± 0.1 to 3.9 ± 0.1 nm^2 PSII^{-1}), followed by a gradual decrease over the next 48 h, after which it reached a minimum at 2.5 ± 0.1 and more or less stabilized at this level until the end of the time course (Fig. 1c; Table S2). The capacity for regulated nonphotochemical quenching (Y(NPQ)) increased slightly from 0.29 ± 0.02 to 0.35 ± 0.02 after 6 h under HL. Between 12 and 24 h, Y(NPQ) declined to its minimum observed (0.14 ± 0.07), before increasing and stabilizing at approximately the initial level (*c.* 0.28;

Fig. 1e; Table S2). Nonregulated nonphotochemical quenching (Y(NO)) displayed opposite trends, with the highest levels (0.84 ± 0.08) being observed after 6 h under HL, before dropping and stabilizing at levels similar to initial LL values ($c.$ 0.66; Fig. 1g; Table S2). The light utilization coefficient α decreased over time as a result of HL exposure: after 1 h of HL exposure, α decreased from 0.25 ± 0.04 to 0.16 ± 0.00 fmol e^- per cell h^{-1} (μmol photons $m^{-2} s^{-1})^{-1}$, where it remained stable until a further gradual decrease from 6 h onwards, reaching lowest values of 0.05 ± 0.00 fmol e^- per cell h^{-1} (μmol photons $m^{-2} s^{-1})^{-1}$ after 72 h of HL exposure. Thereafter, α rose slightly, reaching 0.08 ± 0.02 fmol e^- per cell h^{-1} (μmol photons $m^{-2} s^{-1})^{-1}$ by the end of the time course (Fig. 2a; Table S2). Electron transport rates at $380\ \mu$mol photons $m^{-2} s^{-1}$ (ETR$_{HL}$) showed an initial drop during the first 15 min of HL exposure (from 23 ± 2 to 18 ± 1 fmol e^- per cell h^{-1}), but then increased back to initial levels after 6 h. In line with the response in α, ETR$_{HL}$ dropped more gradually between 6 and 72 h (to 11 ± 1 fmol e^- per cell h^{-1}) before rising to final levels of 19 ± 3 fmol e^- per cell h^{-1} (Fig. 2c; Table S2). The light acclimation index (E_k) increased from $c.\ 100\ \mu$mol photons $m^{-2} s^{-1}$ in LL-acclimated cells to $c.\ 210\ \mu$mol photons $m^{-2} s^{-1}$ after $c.\ 48$ h under HL (Fig. 2e; Table S2). The cellular quotas of light harvesting pigments (Chl$a$, fucoxanthin, Chl$c$ 1 + 2) in $T.\ hyalina$ did not change significantly in response to the HL exposure (Fig. 3a; Table S2). However, when normalized to POC, a significant reduction of 50% in response to HL became evident (Tables S2, S3). The cumulative cellular quota of photoprotective pigments (DD + DT) was significantly elevated after 24 h of HL exposure, but decreased again to values similar to those found under LL by the end of the time course (24.8 ± 6.6 fg per cell; Fig. 3c; Table S2). $T.\ hyalina$'s growth rates, POC and PON quotas, as well as POC production were significantly higher in response to HL (Tables S2, S3).

Numerous transcripts of conventional light-harvesting antennae, mostly of the fucoxanthin/chlorophyll-binding protein (FCP) type, were rapidly and transiently downregulated in response to HL (Fig. 4a,b), while antennae of the protective LI818 type were prominently upregulated (Fig. 4c,d). Also, numerous transcripts related to photosynthetic electron transfer, especially the oxygen-evolving complex and the reaction center protein M of PSII, as well as subunits of the cytochrome b_6/f complex and ferredoxin-NADP$^+$-reductase were transiently downregulated in response to HL exposure. Only a few transcripts (e.g. the D1 protein, the stabilizing psbW subunit of PSII, as well as ferredoxin) were upregulated (Fig. 4e,f). Several transcripts involved in Chl synthesis (Fig. 4g,h) were transiently downregulated due to HL exposure (e.g. coproporphyrinogen III oxidase, Mg-protoporphyrin IX methyltransferase and uroporphyrinogen decarboxylase). Transcripts related to antioxidative protective mechanisms were prominently upregulated in response to HL exposure (Fig. 4i,j), especially of the glutathione system, such as glutaredoxin, glutathione dehydrogenase and a glutathione S-transferase-like protein. Also, several transcripts related to the ascorbate system (e.g. ascorbate peroxidase and dehydroascorbate reductase) were significantly upregulated. One

transcript related to vitamin E synthesis, tocopherol o-methyltransferase, was also upregulated. Few transcripts of carbon metabolism were upregulated, including two transcripts related to the synthesis of mycosporine-like amino acids (2-epi-5-epi-valiolone synthase, Fig. 4k,l). Transcripts related to lipid metabolism, many of which were desaturases (i.e. enzymes that introduce double bonds into acyl-chains), experienced an ambiguous regulation at 2 h, but were concertedly upregulated at 24 h and reverted to near-baseline expression levels after 120 h (Fig. 4m,n).

HL responses in $N.\ frigida$

$Nitzschia\ frigida$ responded faster and more strongly to HL exposure than $T.\ hyalina$, and did not achieve a successful acclimation to elevated light levels within the experiment. F_v/F_m declined from 0.53 ± 0.00 to 0.23 ± 0.03 (i.e. by $c.\ 50\%$) after only 15 min of HL exposure and did not notably recover over the time course (Fig. 1a; Table S2). σ_{PSII} decreased gradually from 4.0 to $2.2\ nm^2\ PSII^{-1}$ over 48 h of HL exposure. Thereafter, no further changes in σ_{PSII} were detectable (Fig. 1c; Table S2). Also Y(NPQ) and Y(NO) showed rapid responses: after only 15 min of HL exposure, Y(NPQ) dropped immediately from 0.45 ± 0.08 to 0.06 ± 0.05 while Y(NO) increased from 0.54 ± 0.09 to 0.92 ± 0.05. With the exception of a small peak in Y(NPQ) and decline in Y(NO) at 24 h, there were no notable changes in these parameters for the rest of the time course (Fig. 1e,g; Table S2). α decreased steadily from 0.09 ± 0.02 fmol e^- per cell h^{-1} (μmol photons $m^{-2} s^{-1})^{-1}$ under LL to 0.01 ± 0.00 fmol e^- per cell h^{-1} (μmol photons $m^{-2} s^{-1})^{-1}$ at the end of the experiment (Fig. 2a; Table S2). ETR$_{HL}$ did not significantly change upon HL exposure (Fig. 2c; Table S2). E_k reached a higher level compared to $T.\ hyalina$ and increased from initially 56 ± 20 to $c.\ 350\ \mu$mol photons $m^{-2} s^{-1}$ (Fig. 2e; Table S2). HL exposure significantly decreased cellular quotas of light-harvesting pigments Chl$a$, fucoxanthin, Chl$c$ 1 + 2 and Chl$c$ 3 (Fig. 3b; Table S2). The cumulative quotas of the protective pigments DD + DT increased significantly after 24 h and beyond, resulting in almost five-fold higher DD + DT quotas in HL-acclimated cells compared to LL-acclimated cells (Fig. 3d). Growth rates of $N.\ frigida$ were significantly lowered as a consequence of HL exposure, while POC and PON quotas as well as POC production remained at levels similar to those of LL-acclimated cells (Tables 2, S3).

In response to HL exposure, $N.\ frigida$ also showed a patterned gene expression response, with transcripts being transiently up- or downregulated before returning to previous expression levels in the course of the experiment. Data revealed that $N.\ frigida$ rapidly downregulated numerous transcripts of light-harvesting proteins of the FCP type (Fig. 4o,p). In contrast to $T.\ hyalina$, however, $c.\ 30$ putative FCP-related light-harvesting proteins were found strongly upregulated. Transcripts related to antennae of the protective LI818 type were prominently upregulated (Fig. 4q,r), as seen in $T.\ hyalina$. Unlike in $T.\ hyalina$, upregulation of transcripts related to the diatom xanthophyll cycle (homologs of zeaxanthin epoxidase,
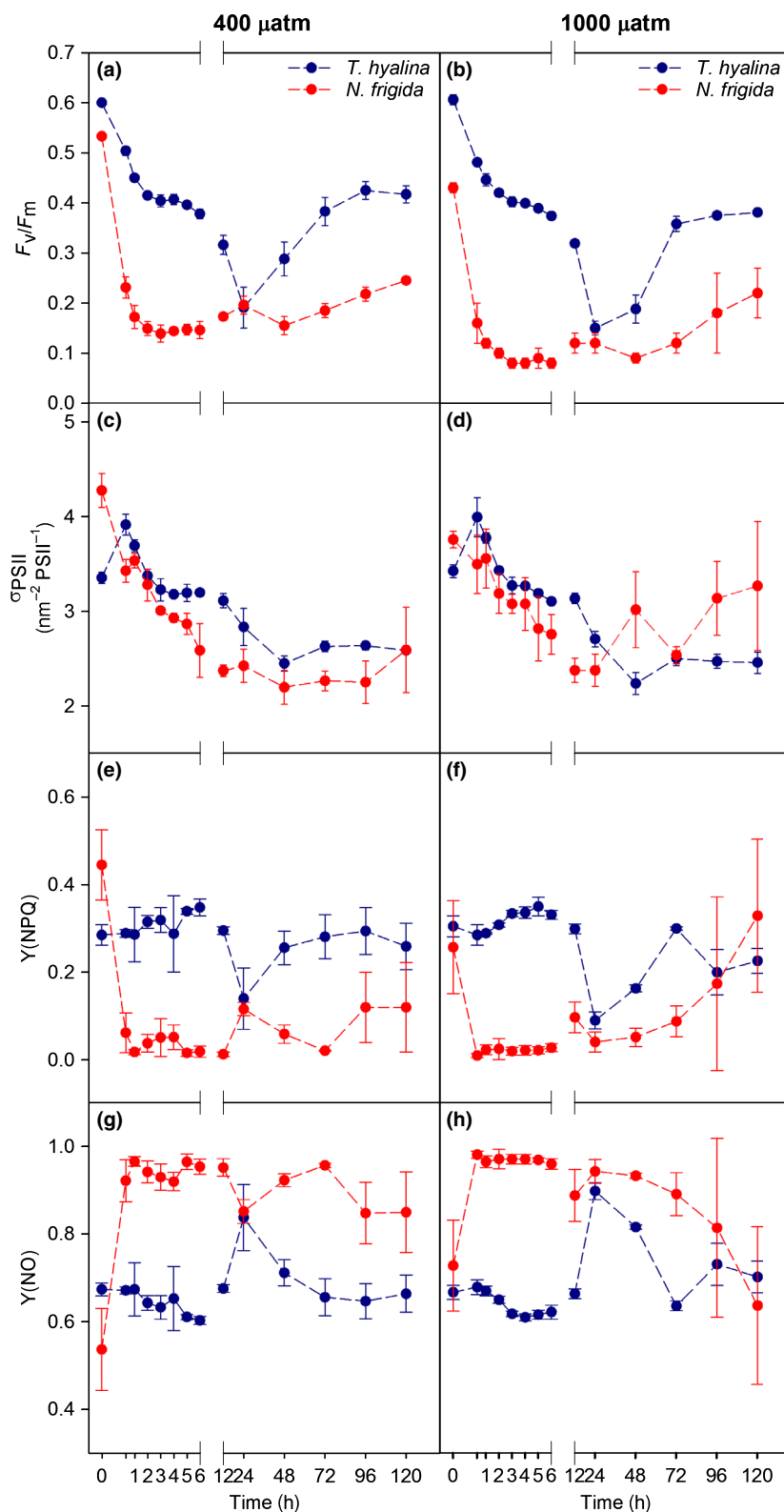
Fig. 1 Temporal changes of dark-acclimated maximum quantum yield of fluorescence (F_v/F_m; a, b), absorption cross-section of photosystem II (σ_{PSII}; c, d), regulated nonphotochemical quenching (Y(NPQ); e, f) and nonregulated nonphotochemical quenching (Y(NO); g, h) in *Thalassiosira hyalina* (blue) and *Nitzschia frigida* (red). Cells were grown at 400 µatm (left panels) and 1000 µatm pCO$_2$ (right panels) under low light (time point 0) and after 1, 2, 3, 4, 5, 6, 12, 24, 48, 72, 96 and 120 h of high light (380 µmol photons m^{-1} s^{-1}) exposure ($n = 3 \pm 1$ SD).
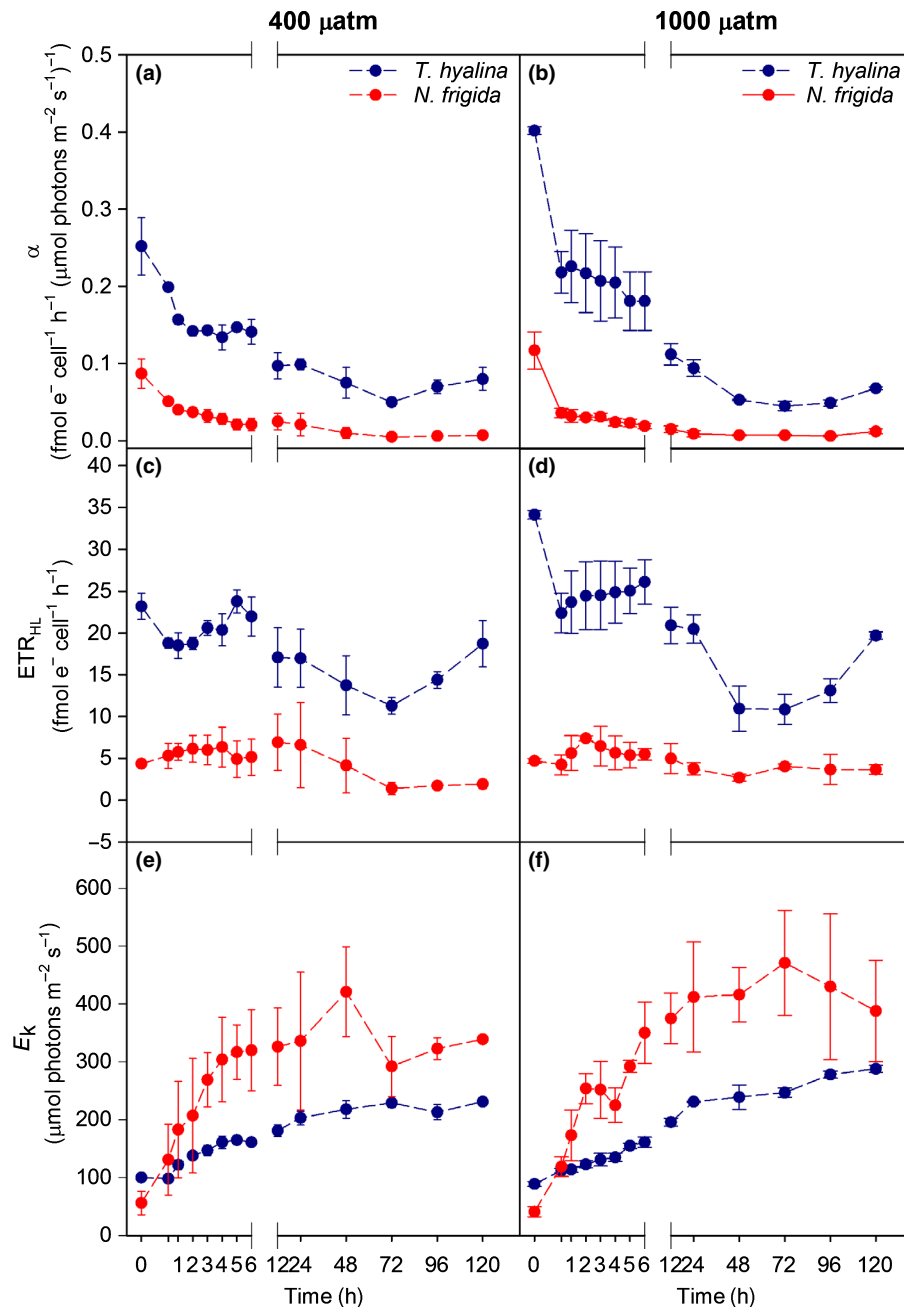
Fig. 2 Temporal changes of light utilization coefficient (α; a, b), relative electron transport rate at applied high light irradiance (ETR$_{HL}$; c, d) and light saturation index (E_k; e, f) in *Thalassiosira hyalina* (blue) and *Nitzschia frigida* (red). Cells were grown at 400 µatm (left panels) and 1000 µatm pCO$_2$ (right panels) under low light (time point 0) and after 1, 2, 3, 4, 5, 6, 12, 24, 48, 72, 96 and 120 h of high light (380 µmol photons m^{-1} s^{-1}) exposure ($n = 3 \pm 1$ SD).

diadinoxanthin de-epoxidase) was detectable. As observed in *T. hyalina*, transcripts related to photosynthetic electron transfer, such as subunits of the oxygen-evolving complex at PSII and reaction center protein psbM, were downregulated, while the psbW and psbP proteins were upregulated (Fig. 4s,t). Transcripts related to the synthesis of chlorophylls were, as in *T. hyalina*, transiently downregulated and gene expression was re-established towards the end of the time course at a slightly higher level (Fig. 4u,v). In response to HL exposure, *N. frigida* slightly upregulated fewer and different transcripts related to

oxidative stress detoxification than *T. hyalina*, in particular two transcripts related to Mn- and Cu/Zn-based superoxide dismutases as well as two transcripts related to vitamin E synthesis (tocopherol polyprenyltransferase-like protein) and membrane protection (probable phospholipid hydroperoxide glutathione peroxidase isoform X1; Fig. 4w,x). In contrast to *T. hyalina*, few transcripts related to the glutathione and ascorbate antioxidant systems were weakly regulated. As in *T. hyalina*, transcripts related to lipid metabolism were ambiguously regulated: several transcripts involved in lipogenesis (e.g. long-chain acyl-CoA
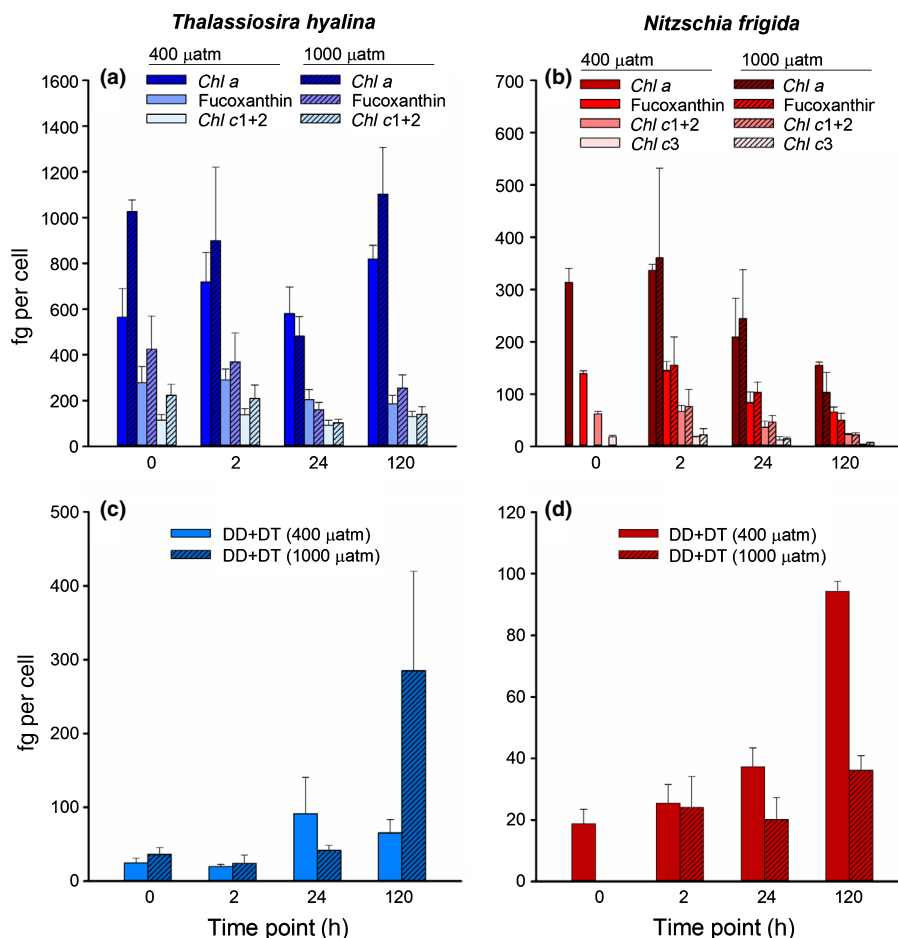
Fig. 3 Light-harvesting pigment quotas (Chl*a*, fucoxanthin, Chl*c* 1 + 2 and Chl*c* 3; a, b) as well as light protective pigment quotas (diadinoxanthin and diatoxanthin, DD + DT; c, d) in *Thalassiosira hyalina* (a, c, blue) and *Nitzschia frigida* (b, d, red) at $p\mathrm{CO_2}$ levels of 400 µatm (without pattern) and 1000 µatm (with pattern). Pigment quotas were analyzed in low light (time point 0) and high light (time point 120) acclimated cells, as well as after 2 h and 24 h of HL exposure (380 µmol photons m^{-1} s^{-1}, $n \geq 3 \pm 1$ SD)

Table 2 Growth rates, cellular quotas of particulate organic carbon and nitrogen (POC/PON) and POC production ($n = 4$; mean $\pm$ 1 SD), in addition to cell size ($n = 30$; mean $\pm$ SD) of *Thalassiosira hyalina* and *Nitzschia frigida* at low light (LL; 20 µmol photons m^{-1} s^{-1}) and high hight (HL; 380 µmol photons m^{-1} s^{-1}) under two $p\mathrm{CO_2}$ levels (400 and 1000 µatm).

Species	Light	$p\mathrm{CO_2}$ (µatm)	Growth rate μ (d^{-1})	POC (pmol per cell)	PON (pmol per cell)	POC production (pmol per cell d^{-1})	Chl*a* : POC (g g^{-1} × 1000)	Cell size (µm)
T. hyalina	LL	400	0.72 ± 0.10^L	24.5 ± 4.9^L	4.4 ± 1.1^L	15.4 ± 0.9^L	2.13 ± 0.18*^{L}	21.6 ± 2.1
T. hyalina	HL	400	0.92 ± 0.10^{LC}	61.8 ± 6.5^L	12.4 ± 1.4^L	59.2 ± 10.6^L	1.11 ± 0.15^L	27.4 ± 2.6
T. hyalina	LL	1000	0.62 ± 0.07	33.6 ± 7.9^L	6.4 ± 1.3^L	23.3 ± 5.5	2.43 ± 0.52*^{L}	20.6 ± 2.5
T. hyalina	HL	1000	0.66 ± 0.14^C	68.3 ± 19.0^L	13.5 ± 3.9^L	44.6 ± 15.7	1.40 ± 0.33^L	26.4 ± 3.0
N. frigida	LL	400	0.26 ± 0.02^C	14.7 ± 1.0	1.8 ± 0.2	3.8 ± 0.2^C	1.79 ± 0.26	7.5 ± 1.0
N. frigida	HL	400	0.22 ± 0.01*	17.0 ± 0.1*	2.2 ± 0.1*	3.9 ± 0.1*^{C}	0.75 ± 0.03*	7.0 ± 1.2
N. frigida	LL	1000	0.37 ± 0.05^{LC}	9.1 ± 1.5	1.3 ± 0.2	3.2 ± 0.3^C	na	5.9 ± 0.6
N. frigida	HL	1000	0.15 ± 0.00*^{L}	31.8 ± 24.4*	4.2 ± 3.4*	2.7 ± 0.8*^{C}	0.50 ± 0.08*	6.7 ± 0.9

*m $n = 3$; mean $\pm$ SD. A superscript L indicates a significant effect of light treatments within a $p\mathrm{CO_2}$ and a superscript C indicates a significant effect of $\mathrm{CO_2}$ levels within a light treatment. na, not available.

synthetase or the acyl carrier protein) were downregulated, while other transcripts, especially those related to desaturases, were upregulated (e.g. precursor of omega-3 desaturase, a generic acyl desaturase, dihydroceramide delta-4 desaturase and delta 9 desaturase; Fig. 4ä,ö).

$p\mathrm{CO_2}$ responses of both species

In *T. hyalina* cultures grown under LL, OA significantly increased light utilization capacity (α) and light-harvesting pigment quota (Chl*a*, fucoxanthin and Chl*c* 1 + 2: Figs 2, 3; Tables S3, S4). Also
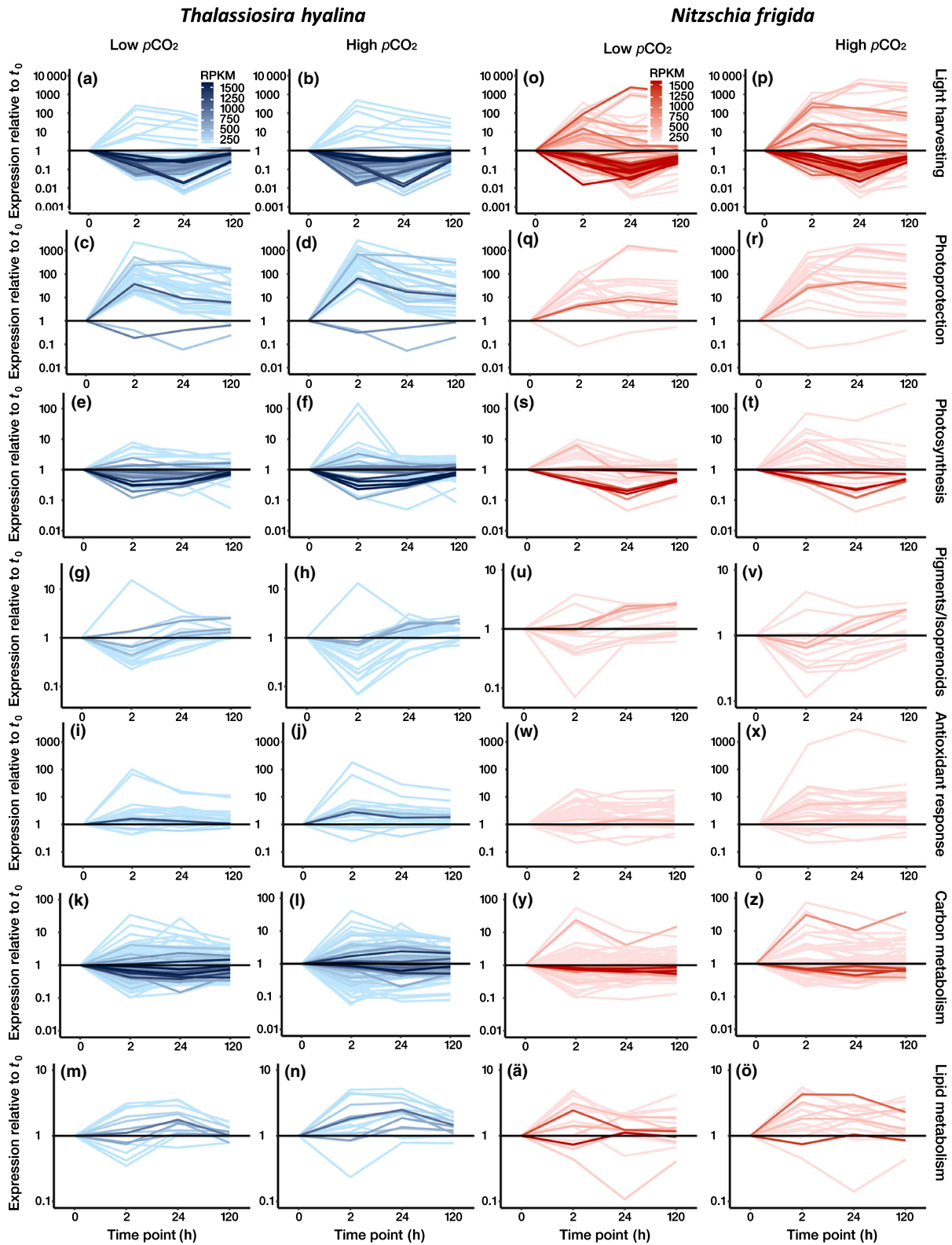
Fig. 4 Time course of expression changes of the identified and classified genes of interest in *Thalassiosira hyalina* (a–n, blue) and *Nitzschia frigida* (o–ö, red) under low (400 µatm; left panels) and high (1000 µatm; right panels) pCO$_2$. Color intensity codes the overall expression levels, based on average numbers of reads per kilobase per million mapped nucleotides (RPKM) across the time course. Labels on the right represent functional classification.

LL-ETR$_{HL}$ was significantly higher in cells grown under 1000 µatm (34 ± 1 fmol e$^-$ per cell h^{-1}) compared to 400 µatm (23 ± 2 fmol e$^-$ per cell h^{-1}, Table S4). This translated to a slightly higher POC

production in cells grown under high (23.3 ± 5.5 pmol per cell d^{-1}) compared to low pCO$_2$ (15.4 ± 0.9 pmol per cell d^{-1}), although this lacked statistical significance. OA did not affect

growth rates under LL conditions (Tables 2, S3). Interestingly, this changed under HL exposure, where differences in α, light-harvesting pigments and ETR_{HL} disappeared and effects on other parameters were observed: F_v/F_m values decreased significantly under OA (Fig. 1a) while DD + DT quotas (Fig. 3c) increased significantly in cells acclimated to HL (Table S4). This translated into significantly lower growth rates under high pCO_2 (0.66 ± 0.14 d^{-1}) compared to low pCO_2 (0.92 ± 0.10 d^{-1}) for HL-acclimated cells (Tables 2, S3). *Nitzschia frigida* responded differently to OA when grown under LL: F_v/F_m decreased significantly (Fig. 1a,b; Table S4), in line with slightly decreased POC production under high vs low pCO_2 (3.2 ± 0.3 vs 3.8 ± 0.2 pmol per cell d^{-1}). At the same time, growth rates increased under OA and LL (Tables 2, S3). Under HL, the pCO_2 responses of *N. frigida* were more similar to those of *T. hyalina,* but led to steeper declines in growth and biomass production in the former.

The gene expression changes in *T. hyalina* and *N. frigida* in response to pCO_2 alone were negligible, and no explicit regulation patterns could be identified in the genes of interest, except that on average, transcript abundance was slightly lower: for *T. hyalina,* the average gene expression under elevated pCO_2 was 0.933, that is the genes of interest experienced *c.* 7% downregulation under elevated pCO_2 (n = 1849, regarding all transcripts with average RPKM ≥ 35; Fig. 5a). Regarding only those genes that could be successfully attributed to physiological processes, the average expression under elevated pCO_2 was 0.905 (n = 998), reflecting a decrease in gene expression of *c.* 10%. Only a negligible 2.5% of classified genes experienced a ≥ 2-fold regulation. In *N. frigida,* the average expression under elevated pCO_2 was 0.972, that is genes experienced *c.* 3% downregulation under elevated pCO_2 (n = 1362, regarding all transcripts with average RPKM ≥ 35; Fig. 5b). Regarding only those genes that could be successfully attributed to physiological processes, the average regulation under elevated pCO_2 was 0.944 (n = 553), reflecting an average decrease in gene expression of only *c.* 5%. The proportion of classified genes that experienced a regulation ≥ 2-fold was 9.6% higher than in *T. hyalina,* but again, the resulting expression patterns did not point towards specific CO_2-sensitive processes.

However, regarding modulation of the HL responses by pCO_2, the data indicated that in *T. hyalina,* those transcripts that were upregulated in response to HL stress generally experienced a stronger upregulation when cells were grown under high pCO_2 (Fig. 5c). When transcripts were downregulated in response to HL stress, this downregulation was on average *less* intense (i.e. dampened by elevated pCO_2; Fig. 5e). In *N. frigida,* this effect was even more apparent, where upregulations due to HL were on average up to *c.* 50-fold stronger under high pCO_2, and downregulations were on average dampened to *c.* 90% of their intensity (Fig. 5d,f).

Discussion

Thalassiosira hyalina showed high resilience against HL stress

Thalassiosira hyalina's response to HL underwent different phases, namely a short-term response (first 12 h), an intermediate

recovery phase (24–72 h) and a re-acclimated state (> 72 h), as observed before for diatoms (Nymark *et al.,* 2009). Such acclimation dynamics were also well reflected in the time-course of gene expression, in which most genes initially showed a strong excursion of expression values (up- or downregulation) and a reversion or re-establishment of a new expression level over the course of acclimation (Figs 4a–ö, S1; Table S7).

In the short-term response phase, *T. hyalina* experienced a fluctuation in active PSIIs, as indicated by changes in F_v/F_m and σ_{PSII} (Fig. 1a,c). A transient initial increase in σ_{PSII} as observed here can occur when the number of active PSII drops faster (evident by the initial drop in F_v/F_m) than the antenna content, and the remaining antenna serves fewer reaction centers, thus increasing σ_{PSII} of the remaining PSII (Wu *et al.,* 2012). Also, an increased xanthophyll cycle-dependent NPQ (Y(NPQ)) was part of this typical diatom response to HL stress (Fig. 1e; Brunet *et al.,* 2011; Giovagnetti & Ruban, 2017) that was recognizable also on the transcriptomic level: cells rapidly decreased expression of conventional fucoxanthin-Chl*a*/*c*-bearing proteins (FCPs; Fig. 4a,b) to reduce light harvesting. Concomitantly, cells induced FCP homologs of the LI818 clade (Fig. 4c,d), thereby leveraging photoprotection by NPQ (Zhu & Green, 2010; Nymark *et al.,* 2013). As a result, active PSII started to recover, as indicated by stabilizing F_v/F_m levels after *c.* 3 h, and σ_{PSII} returned back to initial values (Fig. 1a,c). Beyond this, *T. hyalina* also decreased expression of core components of PSII and the cytochrome b$_6$/f complex to maintain balanced photosynthetic electron transport despite higher excitation pressure. This ability to divert a higher fraction of excitons into harmless dissipation pathways and to accommodate the photosynthetic electron transfer chains was probably one reason for the increasing ETR_{HL} between 1 and 6 h despite HL stress (Fig. 2c). The upregulation of the D1 protein (Fig. 4e,f) reflected the intense 'wear and tear' under HL conditions (Galindo *et al.,* 2017): this protein is highly susceptible to oxidative damage, and its dysfunctional remnants act as inductors of its own gene expression (Tyystjärvi *et al.,* 1996).

Thalassiosira hyalina's intermediate response to HL involved the typical alteration of pigment composition (Brunet *et al.,* 2011). Significantly increased DD + DT quotas after 24 h of HL exposure supported that *T. hyalina* synthesized photoprotective pigments as a countermeasure against the substantial HL stress (Lavaud *et al.,* 2004). Although the expression of enzymes involved in Chl synthesis was decreased at 2 h, recovered around 24 h and re-established at a higher level at 120 h (Fig. 4g,h), the measured cellular light-harvesting pigment quotas did not change significantly over the time course. When normalized to POC, however, a significant reduction in pigmentation was evident between LL- and HL-acclimated cells, which were consistent with an actual drop of light-harvesting capacity per PSII (i.e. σ_{PSII}, Fig. 1c). Remarkably, *T. hyalina* induced numerous genes related to the ascorbate and glutathione antioxidant systems under HL stress (Fig. 4i,j). These dissipate oxidative stress by detoxification of hydrogen peroxide (H_2O_2), the main product of oxygen photoreduction and dismutation (Foyer & Noctor, 2011). The pronounced regulation of these transcripts indicates that these
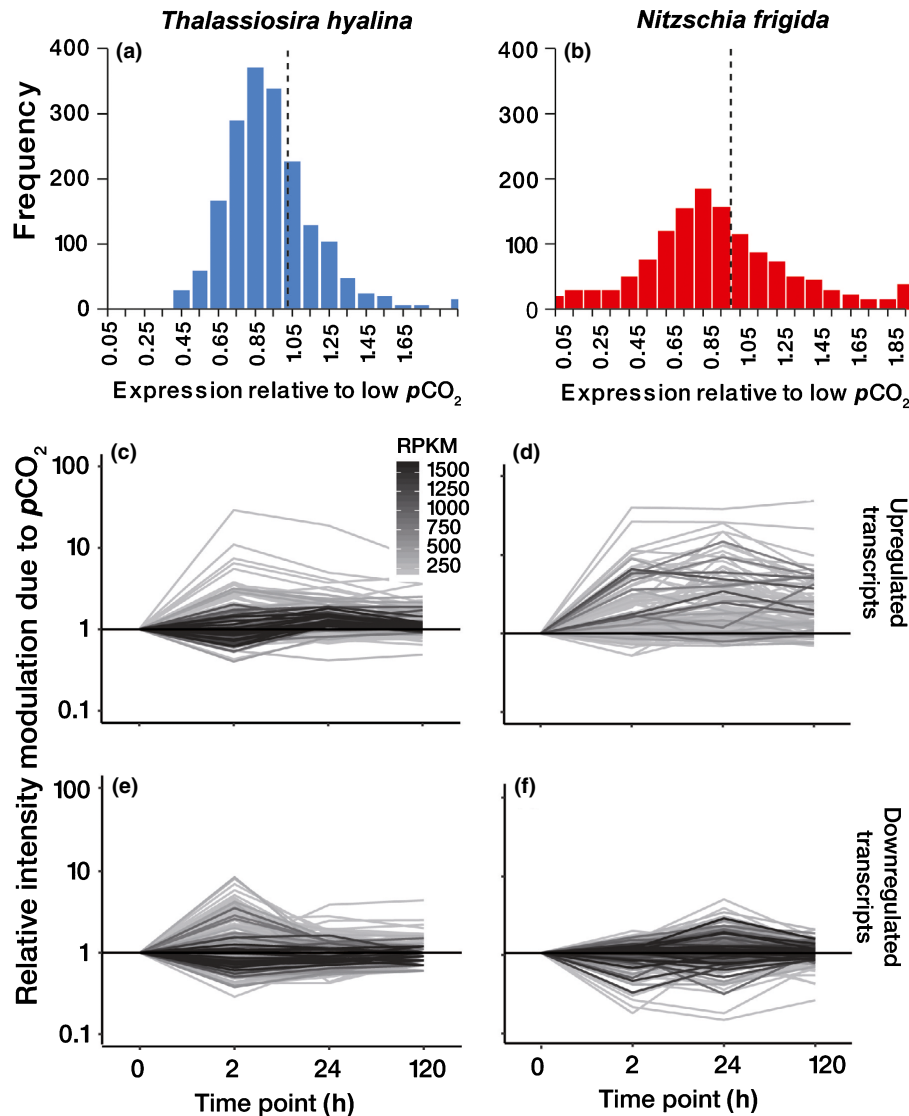
Fig. 5 Histograms representing the expression values of identified and classified transcripts in *Thalassiosira hyalina* (a, blue, $n = 1857$) and *Nitzschia frigida* (b, red, $n = 1358$) in response to elevated pCO_2, where the dashed line represents 1 (i.e. no expression change). (c–f) Graphs showing the time course of pCO_2-mediated relative intensity modulation of the light stress response for upregulated (c, d) and downregulated (e, f) genes in *Thalassiosira hyalina* (left; c, e) and *Nitzschia frigida* (right; d, f). Color intensity codes the overall expression levels, based on averaged numbers of reads per kilobase per million mapped nucleotides (RPKM) across the time courses in both pCO_2 levels.

systems are the prime defenses against oxidative stress in *T. hyalina*. Furthermore, the increased expression of a transcript related to the synthesis of vitamin E, a membrane-situated antioxidant that synergistically cooperates with the ascorbate system (Buettner, 1993), indicates that the avoidance of lipid damage from H_2O_2 is the second major strategy to cope with photophysiological stress. This is in line with the induction of multiple desaturases under HL, which increase the proportions of unsaturated fatty acids in organellar lipid bilayers. Desaturation of lipids causes a higher membrane fluidity, which increases the membrane-mobility of vitamin E and eases the replacement of photosynthetic components (Los *et al.*, 2013). Two of the most prominently upregulated transcripts under HL stress (> 350 fold-change throughout the dataset) map to a 2-epi-5-epi-valiolone synthase-like enzyme, an enzyme involved in the synthesis of

mycosporine-like amino acids. These aromatic molecules are found in all marine algae and protect cells from UV radiation and oxidative stress (Shick & Dunlap, 2002; Wada *et al.*, 2015). These data indicate that *T. hyalina* cells reacted to HL exposure not only with decreased photon harvest and increased NPQ, but counteract oxidative stress with the concerted induction of effective antioxidant systems that are rooted at the 'heart of the cellular redox hub' (Foyer & Noctor, 2011). Furthermore, these findings corroborate that photosynthesis as a whole is a sensory–autoregulatory process (Pfannschmidt, 2003) and that redox-balance is its major regulator (Mittler, 2002; Stenbaek & Jensen, 2010). Despite the ability to cope well with photooxidative stress in the short term, several key variables reached minimal values during the course of the experiment between the 24 and 72 h time points (F_v/F_m, σ_{PSII}, Y(NPQ), α and ETR_{HL}; Figs 1, 2).

Beyond 72 h, *T. hyalina* entered the re-acclimation phase in which the operability of the photosynthetic machinery recovered, and F_v/F_m, Y(NPQ), α and ETR_{HL} increased, with E_k having approached the HL intensity used in the experiments (Figs 1, 2). HL-acclimated cells also increased in size, in line with higher POC quotas compared to LL (Table 2), which appears to be a common response of many phytoplankton species towards high irradiances (Thompson *et al.*, 1991). The increase in cell size also explains why cell-normalized light harvesting pigment quotas in HL were not lower than in LL, as would be expected after acclimation to higher irradiances. This became evident in the biomass-normalized pigment quotas, which decreased by more than 50% in response to HL. These adjustments of the photosynthetic machinery, as discussed above, facilitated highly effective photosynthesis in HL-acclimated *T. hyalina* cells, as indicated by significantly higher growth rate and almost four times higher POC production (Table 2).

Nitzschia frigida exhibited higher sensitivity towards light stress

The short-term responses of *N. frigida* in the first 12 h were clearly different from those of *T. hyalina*. While a 50% reduction in F_v/F_m of *T. hyalina* was observed after 12 h of HL exposure compared to the initial LL conditions, an equivalent reduction was evident after only 15 min under HL in *N. frigida* (Fig. 1a). Similarly, energy partitioning between Y(NPQ) and Y(NO) in *N. frigida* was also different and exhibited a more extreme short-term response to HL compared to *T. hyalina*: within the first 15 min of HL exposure, Y(NPQ) dropped from 0.45 ± 0.08 to 0.06 ± 0.05 concomitantly with an increase of Y(NO) from 0.54 ± 0.09 to 0.92 ± 0.05 (Fig. 1e,g). Such light-dependent increases in Y(NO) have been observed earlier in other psychrophilic ('cold-living') species such as Antarctic *Chlamydomonas raudensis* strain UWO 241 (Szyszka *et al.*, 2007) and the Arctic diatom *Chaetoceros neogracilis* (Lacour *et al.*, 2019). This could indicate that psychrophilic species prefer xanthophyll cycle-independent energy dissipation Y(NO), such as PSII reaction center quenching, rather than light harvesting complex II xanthophyll cycle-dependent energy dissipation, Y(NPQ) (Ivanov *et al.*, 2008). Under very low F_v/F_m (< 0.15) as seen is this study, however, the high values of Y(NO) more likely reflect the cells' inability to compensate for damage by excess illumination (Klughammer & Schreiber, 2008), which leads to increasing levels of deactivated reaction centers. Moreover, *N. frigida* exhibited consistently decreasing σ_{PSII} from the start (Fig. 1c), without a transient peak, indicating a fundamental collapse of light-harvesting capacity per PSII, consistent with a drop in α (Fig. 2a) and the quotas of light-harvesting pigments (Fig. 3b). Like *T. hyalina*, *N. frigida* downregulated conventional FCPs (Fig. 4o, p) and upregulated photoprotective LI818 homologs (Fig. 4q,r). However, *c.* 30 conventional FCPs were upregulated, which probably hampered the cells' attempt to reduce photon harvest to the possible minimum. Also, *N. frigida* downregulated components of PSII to decrease overall electron harvest, but the downregulation of ferredoxin-NADP$^+$-reductase (Fig. 4s,t), typically

the terminal enzyme of photosynthetic light reactions, seemingly impaired electron drainage (Hartmann *et al.*, 2014). This explains the constantly high turnover times of the electron transfer chain (τ_{ES}, Fig. S2). Unlike *T. hyalina*, *N. frigida* did not prominently induce the ascorbate- and glutathione-related antioxidant systems, but rather weakly upregulated comparably few transcripts of Mn- as well as Cu/Zn-based superoxide dismutases (Fig. 4w,x), which catalyze the conversion of superoxide radicals into H_2O_2. The different indicated metal cofactors suggest that the regulated enzymes have different organellar location, and because oxidative stress regulates gene expression of antioxidant systems (Mittler, 2002), *N. frigida* apparently experienced oxidative stress in all major cellular compartments. The increased expression of a tocopherol polyprenyltransferase-like protein and a probable phospholipid hydroperoxide glutathione peroxidase (Fig. 4w,x) suggests that *N. frigida* also attempted to protect organellar membranes from oxidative stress and dangerous lipid-peroxidizing chain reactions (Pospíšil & Yamamoto, 2017). In line with this, *N. frigida* induced numerous desaturases (Fig. 4ä,ö). As in *T. hyalina*, these served to increase fluidity in lipid bilayers, assisting repair of enzymatic machinery, enhancing the scavenging of oxidative stress by membrane-situated antioxidants, and creating unsaturated lipids that act as quenchers of oxidative stress themselves (Richard *et al.*, 2008; Los *et al.*, 2013).

Throughout the experiment, *N. frigida* did not achieve a proper acclimation to HL, experiencing considerable stress and dysfunctional photosynthesis even after 120 h. By that time, the light-harvesting pigment quotas had halved under HL compared to LL, despite *de novo* synthesis of photoprotective pigments at 120 h (Fig. 3b,d). *Nitzschia frigida* did not show any recovery of the photosynthetic parameters F_v/F_m and Y(NPQ) while its Y(NO) remained high, indicating that photoacclimative efforts were insufficient (Figs 1, 2; Klughammer & Schreiber, 2008). As a consequence, growth rates were lowered and POC production could not profit from HL (Table 2). The continuous electron input and concomitant oxidative stress might have contributed to the strong decreases in growth rate under HL. In conclusion, the combination of its high sensitivity to photodamage and the lacking capacity to detoxify oxidative stress seem to have prevented successful recovery and proper acclimation to HL in *N. frigida*. A clearly negative impact of high natural irradiances on sea ice algal communities has been documented previously (Juhl & Krembs, 2010; Leu *et al.*, 2010; A. C. Kvernvik *et al.*, unpublished). However, Juhl & Krembs (2010) estimated that the minimum acclimation time required by sea ice algae took 3–6 d, which was later confirmed by Alou-Font *et al.*, (2013). Whether successful acclimation could be established on longer time scales than in our study (5 d) or more gradual increases in irradiance remains to be tested.

Although the striking differences between the photoacclimative capacities of *T. hyalina* and *N. frigida* were surprising, they could in part be attributed to morphological differences between the species (size and/or shape), that were chosen based on their ecological dominance in the respective habitats. Small pennate diatoms (e.g. *N. frigida*) have larger surface-to-volume quotients compared to larger centric diatoms (e.g. *T. hyalina*), the latter

typically showing lower intrinsic susceptibility to photo-inactivation in response to short-term HL exposure (Key *et al.*, 2010). This is hypothesized to be due to lower light-harvesting capacity per PSII and maximum metabolic rates compared to smaller cells (Lavaud *et al.*, 2007; Key *et al.*, 2010; Fig. 1c). Centric diatoms were also found to be able to outcompete pennate diatoms in situations with relatively high irradiances (thin snow cover and/or ice), which could indicate that centrics have a competitive advantage under higher light availability compared to pennates also within one habitat type (Melnikov *et al.*, 2002; Campbell *et al.*, 2018). In addition to their variation in size and shape, clear differences in photoacclimative capacity between *T. hyalina* and *N. frigida* may also be attributed to the habitats and ecological niches these two species are adapted to. Reported light transmittance through ice and snow layers is often very low (Leu *et al.*, 2010; Assmy *et al.*, 2017; Hancke *et al.*, 2018), so that sympagic algae usually experience gradually changing irradiances with low amplitude as snow and ice melt (Hill *et al.*, 2018). Vertical mixing of phytoplankton cells in open water, by contrast, causes fluctuating light intensities at short time scales and high amplitudes (MacIntyre *et al.*, 2000). It can therefore be assumed that pelagic phytoplankton species (such as *T. hyalina*) have adapted to larger irradiance variability on short temporal scales, and are therefore better suited to deal with rapid increases in light than sympagic species (e.g. Behrenfeld *et al.*, 1998).

Light responses were modulated by ocean acidification

In *T. hyalina* cultures grown under LL, OA appeared to be neutral to moderately beneficial. Light utilization increased, as evident by higher α and light-harvesting pigments, which translated into higher ETR_{HL} and slightly higher POC production in cells grown under OA conditions (Figs 2, 3). Increasing seawater pCO_2 levels may increase diffusive carbon uptake and thus lower the energy and resource requirements for CCM operations, which could allow for increased rates of photosynthesis (Raven *et al.*, 2011; Bach & Taucher, 2019). Under HL, however, a significant reduction in growth rates was observed in response to high pCO_2, while beneficial effects on photophysiology disappeared (Table 2; Fig. 2). Together with a significant increase in quotas of xanthophyll cycle pigments and a decrease in F_v/F_m (Figs 2, 3), this indicates higher susceptibility towards HL stress under OA, a negative synergistic interaction that has been observed in several instances before (Gao *et al.*, 2012; McCarthy *et al.*, 2012; Hoppe *et al.*, 2015, 2017). The oxidative stress derived from HL exposure and the concomitant increase of $[CO_2]$ and/or H^+ levels seems to impair overall cellular homeostasis, making it more difficult for cells to maintain or adjust redox balance (Rokitta *et al.*, 2012; Bach *et al.*, 2013). Thus, it may be interpreted that the generally wide CO_2 niche of *T. hyalina* becomes slightly narrower under HL.

Contrary to *T. hyalina*, *N. frigida* seemed to be more negatively affected by OA irrespective of the irradiance level: cells grown under high pCO_2 showed lower F_v/F_m and α, which translated into lower POC production under OA irrespective of light level (Figs 1, 2a,b; Table 2). Regarding growth rates, OA caused

beneficial effects under LL but detrimental effects under HL (Table 2). Despite the fact that growth rate and POC production seem to be affected differently (i.e. have differently shaped reaction norms), this indicates a narrower CO_2 niche of *N. frigida* compared to *T. hyalina*, which is constricted even further by HL. It seems plausible that in *N. frigida* cells, low pH caused distorted ion homeostasis and signaling (Rokitta *et al.*, 2012), which might have additionally hampered re-acclimation. The effects of rising CO_2 and H^+ levels thus seem to be species-specific, which may be due to different tipping points between positive effects of increased CO_2, and negative effects of enhanced H^+ levels (Li *et al.*, 2019). Similar to the responses to HL, differently sized cells have been hypothesized to have different responses to rising pCO_2 levels (e.g. Bach & Taucher, 2019). Wu *et al.* (2014) demonstrated a positive relationship between cell volume and the magnitude of CO_2 fertilization on diatom growth rates, presumably due to higher restriction by diffusion gradients. This agrees well with our observation that *T. hyalina* with its lower surface-to-volume quotient benefits more from OA compared to *N. frigida*, especially under LL conditions.

The effects of OA on the gene expression patterns of both species were ambiguous with respect to biochemical pathways and cellular functions, which is in line with an absence of concrete pCO_2 effects in pelagic assemblages from diverse Arctic habitats (Hoppe *et al.*, 2018). More importantly, the changes of gene expression induced by elevated pCO_2 were so small that an evaluation was pointless: given the applied experimental set-up, replication and sequencing depth, it would require changes > 2-fold to make any reliable statements (Conesa *et al.*, 2016), which was the case for only 2.5% or 9.6% of the data of *T. hyalina* or *N. frigida*, respectively (Fig. 5a,b). Thus, it can only be said that high pCO_2 seemingly lowered the 'on average' expression of light-stress-relevant transcripts across the dataset, an effect that appears to be stronger in *T. hyalina* (on average 10% lower expression under high pCO_2) than in *N. frigida* (on average 5% lower expression under high pCO_2).

The pCO_2 modulation of transcriptomic HL responses was similarly ambiguous. In both species, elevated pCO_2 modulated the HL responses to be on average stronger for upregulated genes and weaker for downregulated genes (Fig. 5c–f). This especially holds true for the majority of the upregulated photoprotective antennae of the LI818 type, the transcripts related to mycosporine-like amino acid synthesis, as well as for the downregulated FCP-like light-harvesting antennae, which explains why the photoprotective responses (e.g. Y(NPQ) of *N. frigida* and photoprotective pigment quotas of *T. hyalina*) under HL and OA are more pronounced. With concrete transcriptomic effects being absent, it seems likely that OA modulation of HL responses manifests through secondary effects on the cells, possibly by altering the *in vivo* substrate availabilities and chemical conditions within or between organelles, or by affecting physiological signals such as membrane potentials or redox equilibria (Rokitta *et al.*, 2012). Thus, despite the species' different capacities to cope with HL stress, OA seems to impose an additional stress that requires more intense regulatory efforts. While this phenomenon did not change the overall picture gained from the

two physiologically and evolutionarily distinct microalgae used here, future environmental change, especially the combination of HL stress and OA, is likely to negatively affect the ecological performance of microalgae and restrict habitat occupation and niche partitioning in the Arctic.

Conclusion

Thalassiosira hyalina, with its robust light-harvesting apparatus and efficient antioxidant systems, handled photophysiological stress well and acclimated rapidly to higher irradiances, leading to increased growth rates and organic carbon quotas under HL conditions. In *N. frigida*, by contrast, photochemical damage and oxidative stress appeared to overpower cellular defenses, causing dysfunctional photophysiology and reduced fitness with decreased photosynthetic yields and growth rates. OA increased these sensitivities to HL stress in both species, highlighting the importance of studying interacting environmental variables together. Despite the overarching nature of these interactions, we found substantial differences in sensitivity between pelagic and sympagic diatoms, which could significantly alter their relative contribution to biomass and annual primary production in a future Arctic. *Thalassiosira hyalina* will probably continue to be a major primary producer in the pelagic realm, which is furthermore becoming more prevalent (Stroeve & Notz, 2018). Due to the increasing importance of ephemeral, that is melting and re-forming sea ice (Onarheim *et al.*, 2018), environmental dynamics encountered by sympagic algae may become more similar to what pelagic organisms experience. Our results indicate a decrease in fitness of important pennate sea-ice algae in response to climate change, potentially altering colonization and productivity in Arctic sea ice with negative effects on downstream food webs. Their differential sensitivity towards climate change needs to be incorporated into scenarios of future Arctic algae blooms, including implications for the ecosystem.

Author contributions

ACK, EL, BR, SDR and CJMH initially planned the experimental approach; ACK and CJMH conducted lab cultivations and collected samples; ACK processed and evaluated the FRRf, pigment and elemental data. SDR processed RNA samples, conducted the sequencing, and processed and evaluated the data; LH assembled the *de novo* transcriptome and assisted in bioinformatical post-processing; ACK and SDR drafted the manuscript; ACK, EL, BR, SDR, CJMH, LH and TMG contributed to writing the final manuscript. ACK and SDR contributed equally to this work.

ORCID

Tove M. Gabrielsen (iD) https://orcid.org/0000-0001-5801-4569
Lars Harms (iD) https://orcid.org/0000-0001-7620-0613
Clara J. M. Hoppe (iD) https://orcid.org/0000-0002-2509-0546
Ane C. Kvernvik (iD) https://orcid.org/0000-0002-7678-5233
Eva Leu (iD) https://orcid.org/0000-0002-5328-3396
Sebastian D. Rokitta (iD) https://orcid.org/0000-0002-7540-9033
Björn Rost (iD) https://orcid.org/0000-0001-5452-5505

References

Aletsee L, Jahnke J. 1992. Growth and productivity of the psychrophilic marine diatoms *Thalassiosira antarctica* Comber and *Nitzschia frigida* Grunow in batch cultures at temperatures below the freezing point of sea water. *Polar Biology* **11**: 643–647.

Alou-Font E, Mundy CJ, Roy S, Gosselin M, Agustí S. 2013. Snow cover affects ice algal pigment composition in the coastal Arctic ocean during spring. *Marine Ecology Progress Series* **474**: 89–104.

Alou-Font E, Roy S, Agustí S, Gosselin M. 2016. Cell viability, pigments and photosynthetic performance of Arctic phytoplankton in contrasting ice-covered and open-water conditions during the spring-summer transition. *Marine Ecology Progress Series* **543**: 89–106.

Altschul SF, Gish W, Miller W, Myers EW, Lipman DJ. 1990. Basic local alignment search tool. *Journal of Molecular Biology* **215**: 403–410.

AMAP. 2018. *Arctic Ocean Acidification Assessment: 2018 Summary for Policymakers.* Oslo, Norway: Arctic Monitoring and Assessment Programme (AMAP).

Andrew S. 2010. FastQC: A quality control tool for high throughput sequence data. [WWW document] URL http://www.bioinformatics.babraham.ac.uk/projects/fastqc

Assmy P, Fernández-Méndez M, Duarte P, Meyer A, Randelhoff A, Mundy CJ, Olsen LM, Kauko HM, Bailey A, Chierici M *et al.* 2017. Leads in Arctic pack ice enable early phytoplankton blooms below snow-covered sea ice. *Scientific Reports* **7**: 40850.

Bach LT, Mackinder LC, Schulz KG, Wheeler G, Schroeder DC, Brownlee C, Riebesell U. 2013. Dissecting the impact of CO_2 and pH on the mechanisms of photosynthesis and calcification in the coccolithophore *Emiliania huxleyi*. *New Phytologist* **199**: 121–134.

Bach LT, Taucher J. 2019. CO_2 effects on diatoms: a synthesis of more than a decade of ocean acidification experiments with natural communities. *Ocean Science* **15**: 1159–1175.

Behrenfeld MJ, Prasil O, Kolber ZS, Babin M, Falkowski PG. 1998. Compensatory changes in photosystem II electron turnover rates protect photosynthesis from photoinhibition. *Photosynthesis Research* **58**: 259–268.

Benjamini Y, Hochberg Y. 1995. Controlling the false discovery rate – a practical and powerful approach to multiple testing. *Journal of the Royal Statistical Society Series B-Methodological* **57**: 289–300.

Brunet C, Johnsen G, Lavaud J, Roy S. 2011. Pigments and photoacclimation processes. In: Roy S, Llewellyn CA, Egeland ES, Johnsen G, eds. *Phytoplankton pigments: characterization, chemotaxonomy and applications in oceanography*. Cambridge, UK: Cambridge University Press, 445–454.

Buettner GR. 1993. The pecking order of free radicals and antioxidants: lipid peroxidation, α-tocopherol, and ascorbate. *Archives of Biochemistry and Biophysics* **300**: 535–543.

Bushnell B. 2015. BBMap short read aligner, and other bioinformatic tools. [WWW document] URL http://sourceforge.net/projects/bbmap

Campbell K, Mundy CJ, Belzile C, Delaforge A, Rysgaard S. 2018. Seasonal dynamics of algal and bacterial communities in Arctic sea ice under variable snow cover. *Polar Biology* **41**: 41–58.

IPCC 2014. Summary for policymakers. In: Field CB, Barros VR, Dokken DJ, Mach KJ, Mastrandrea MD, Bilir TE, Chatterjee M, Ebi KL, Estrada YO, Genova RC, Girma B, Kissel ES, Levy AN, MacCracken S, Mastrandrea PR, White LL, eds. *Climate Change 2014: Impacts, Adaptation, and Vulnerability. Part A: Global and Sectoral Aspects.* Contribution of Working Group II to the Fifth Assessment Report of the Intergovernmental Panel on Climate Change. Cambridge, UK, and New York, NY, USA: Cambridge University Press, 1–32.

Conesa A, Madrigal P, Tarazona S, Gomez-Cabrero D, Cervera A, McPherson A, Szcześniak MW, Gaffney DJ, Elo LL, Zhang X et al. 2016. A survey of best practices for RNA-seq data analysis. *Genome Biology* **17**: 13.

Dickson AG. 1981. An exact definition of total alkalinity and a procedure for the estimation of alkalinity and total inorganic carbon from titration data. *Deep Sea Research Part A. Oceanographic Research Papers* **28**: 609–623.

Eilers PHC, Peeters JCH. 1988. A model for the relationship between light intensity and the rate of photosynthesis in phytoplankton. *Ecological Modelling* **42**: 199–215.

Foyer CH, Noctor G. 2011. Ascorbate and glutathione: the heart of the redox hub. *Plant Physiology* **155**: 2–18.

Galindo V, Gosselin M, Lavaud J, Mundy CJ, Else B, Ehn J, Babin M, Rysgaard S. 2017. Pigment composition and photoprotection of Arctic sea ice algae during spring. *Marine Ecology Progress Series* **585**: 49–69.

Gao K, Campbell DA. 2014. Photophysiological responses of marine diatoms to elevated CO_2 and decreased pH: a review. *Functional Plant Biology* **41**: 449–459.

Gao K, Xu J, Gao G, Li Y, Hutchins DA, Huang B, Wang L, Zheng Y, Jin P, Cai X et al. 2012. Rising CO_2 and increased light exposure synergistically reduce marine primary productivity. *Nature Climate Change* **2**: 519–523.

Giordano M, Beardall J, Raven JA. 2005. CO_2 concentrating mechanisms in algae: mechanisms, environmental modulation, and evolution. *Annual Review of Plant Biology* **56**: 99–131.

Giovagnetti V, Ruban AV. 2017. Detachment of the fucoxanthin chlorophyll a/c binding protein (FCP) antenna is not involved in the acclimative regulation of photoprotection in the pennate diatom *Phaeodactylum tricornutum*. *Biochimica et Biophysica Acta-Bioenergetics* **1858**: 218–230.

Grabherr MG, Haas BJ, Yassour M, Levin JZ, Thompson DA, Amit I, Adiconis X, Fan L, Raychowdhury R, Zeng Q et al. 2011. Full-length transcriptome assembly from RNA-Seq data without a reference genome. *Nature Biotechnology* **29**: 644.

Gradinger R. 2009. Sea-ice algae: major contributors to primary production and algal biomass in the Chukchi and Beaufort Seas during May/June 2002. *Deep Sea Research Part II: Topical Studies in Oceanography* **56**: 1201–1212.

Guillard RR, Ryther JH. 1962. Studies of marine planktonic diatoms: I. *Cyclotella nana* Hustedt, and *Detonula confervacea* (Cleve) Gran. *Canadian Journal of Microbiology* **8**: 229–239.

Hancke K, Lund-Hansen LC, Lamare ML, Højlund Pedersen S, King MD, Andersen P, Sorrell BK. 2018. Extreme low light requirement for algae growth underneath sea ice: a case study from station Nord, NE Greenland. *Journal of Geophysical Research: Oceans* **123**: 985–1000.

Hartmann P, Béchet Q, Bernard O. 2014. The effect of photosynthesis time scales on microalgae productivity. *Bioprocess and Biosystems Engineering* **37**: 17–25.

Hasholt B, Bobrovitskaya N, Bogen J, McNamara J, Mernild SH, Milburn D, Walling DE. 2006. Sediment transport to the Arctic Ocean and adjoining cold oceans. *Hydrology Research* **37**: 413–432.

Hegseth EN, Sundfjord A. 2008. Intrusion and blooming of Atlantic phytoplankton species in the high Arctic. *Journal of Marine Systems* **74**: 108–119.

Hill VJ, Light B, Steele M, Zimmerman RC. 2018. Light availability and phytoplankton growth beneath arctic sea ice: integrating observations and modeling. *Journal of Geophysical Research: Oceans* **123**: 3651–3667.

Hopkinson BM, Dupont CL, Allen AE, Morel FMM. 2011. Efficiency of the CO_2-concentrating mechanism of diatoms. *Proceedings of the National Academy of Sciences, USA* **108**: 3830–3837.

Hoppe CJM, Holtz L-M, Trimborn S, Rost B. 2015. Ocean acidification decreases the light-use efficiency in an Antarctic diatom under dynamic but not constant light. *New Phytologist* **207**: 159–171.

Hoppe CJ, Schuback N, Semeniuk DM, Maldonado MT, Rost B. 2017. Functional redundancy facilitates resilience of subarctic phytoplankton assemblages toward ocean acidification and high irradiance. *Frontiers in Marine Science* **4**: 229.

Hoppe CJM, Wolf KKE, Schuback N, Tortell PD, Rost B. 2018. Compensation of ocean acidification effects in Arctic phytoplankton assemblages. *Nature Climate Change* **8**: 529–533.

Hughes DJ, Campbell DA, Doblin MA, Kromkamp JC, Lawrenz E, Moore CM, Oxborough K, Prášil O, Ralph PJ, Alvarez MF et al. 2018. Roadmaps and detours: Active chlorophyll-a assessments of primary productivity across marine and freshwater systems. *Environmental Science & Technology* **52**: 12039–12054.

Ivanov AG, Sane PV, Hurry V, Öquist G, Huner NP. 2008. Photosystem II reaction centre quenching: mechanisms and physiological role. *Photosynthesis Research* **98**: 565.

Juhl AR, Krembs C. 2010. Effects of snow removal and algal photoacclimation on growth and export of ice algae. *Polar Biology* **33**: 1057–1065.

Key T, McCarthy A, Campbell DA, Six C, Roy S, Finkel ZV. 2010. Cell size trade-offs govern light exploitation strategies in marine phytoplankton. *Environmental Microbiology* **12**: 95–104.

Klughammer C, Schreiber U. 2008. Complementary PS II quantum yields calculated from simple fluorescence parameters measured by PAM fluorometry and the saturation pulse method. *PAM Application Notes* **1**: 27–35.

Kopylova E, Noé L, Touzet H. 2012. SortMeRNA: fast and accurate filtering of ribosomal RNAs in metatranscriptomic data. *Bioinformatics* **28**: 3211–3217.

Kroeker KJ, Kordas RL, Crim R, Hendriks IE, Ramajo L, Singh GS, Duarte CM, Gattuso JP. 2013. Impacts of ocean acidification on marine organisms: quantifying sensitivities and interaction with warming. *Global Change Biology* **19**: 1884–1896.

Lacour T, Morin P-I, Sciandra T, Donaher N, Campbell DA, Ferland J, Babin M. 2019. Decoupling light harvesting, electron transport and carbon fixation during prolonged darkness supports rapid recovery upon re-illumination in the Arctic diatom *Chaetoceros neogracilis*. *Polar Biology* **42**: 1787–1799.

Lavaud J, Goss R. 2014. The peculiar features of non-photochemical fluorescence quenching in diatoms and brown algae. In: Demmig-Adams B, Garab G, Adams III W, Govindjee, eds. *Non-photochemical quenching and energy dissipation in plants, algae and cyanobacteria*. Dordrecht, the Netherlands: Springer, 421–443.

Lavaud J, Rousseau B, Etienne AL. 2004. General features of photoprotection by energy dissipation in planktonic diatoms (Bacillariophyceae). *Journal of Phycology* **40**: 130–137.

Lavaud J, Strzepek RF, Kroth PG. 2007. Photoprotection capacity differs among diatoms: possible consequences on the spatial distribution of diatoms related to fluctations in the underwater light climate. *Limnology and Oceanography* **52**: 1188–1194.

Leu E, Mundy C, Assmy P, Campbell K, Gabrielsen T, Gosselin M, Juul-Pedersen T, Gradinger R. 2015. Arctic spring awakening–Steering principles behind the phenology of vernal ice algal blooms. *Progress in Oceanography* **139**: 151–170.

Leu E, Wiktor J, Søreide J, Berge J, Falk-Petersen S. 2010. Increased irradiance reduces food quality of sea ice algae. *Marine Ecology Progress Series* **411**: 49–60.

Li G, Campbell DA. 2013. Rising CO_2 interacts with growth light and growth rate to alter photosystem II photoinactivation of the coastal diatom *Thalassiosira pseudonana*. *PLoS ONE* **8**: e55562.

Li W, Ding J, Li F, Wang T, Yang Y, Li Y, Campbell DA, Gao K. 2019. Functional responses of smaller and larger diatoms to gradual CO_2 rise. *Science of the Total Environment* **680**: 79–90.

Light B, Perovich DK, Webster MA, Polashenski C, Dadic R. 2015. Optical properties of melting first-year Arctic sea ice. *Journal of Geophysical Research: Oceans* **120**: 7657–7675.

Los DA, Mironov KS, Allakhverdiev SI. 2013. Regulatory role of membrane fluidity in gene expression and physiological functions. *Photosynthesis Research* **116**: 489–509.

MacIntyre HL, Kana TM, Geider RJ. 2000. The effect of water motion on short-term rates of photosynthesis by marine phytoplankton. *Trends in Plant Science* **5**: 12–17.

McCarthy A, Rogers SP, Duffy SJ, Campbell DA. 2012. Elevated carbon dioxide differentially alters the photophysiology of *Thalassiosira pseudonana* (Bacillariophyceae) and *Emiliania huxleyi* (Haptophyta). *Journal of Phycology* **48**: 635–646.

McMinn A. 2017. Reviews and syntheses: Ice acidification, the effects of ocean acidification on sea ice microbial communities. *Biogeosciences* **14**: 3927.

McMinn A, Müller MN, Martin A, Ryan KG. 2014. The response of Antarctic sea ice algae to changes in pH and CO_2. *PLoS ONE* **9**: e86984.

Melnikov IA, Kolosova EG, Welch HE, Zhitina LS. 2002. Sea ice biological communities and nutrient dynamics in the Canada Basin of the Arctic Ocean. *Deep Sea Research Part I: Oceanographic Research Papers* **49**: 1623–1649.

Mittler R. 2002. Oxidative stress, antioxidants and stress tolerance. *Trends in Plant Science* **7**: 405–410.

Mortazavi A, Williams BA, McCue K, Schaeffer L, Wold B. 2008. Mapping and quantifying mammalian transcriptomes by RNA-Seq. *Nature Methods* **5**: 621.

Nicolaus M, Katlein C, Maslanik J, Hendricks S. 2012. Changes in Arctic sea ice result in increasing light transmittance and absorption. *Geophysical Research Letters* **39**: L24501.

Nymark M, Valle KC, Brembu T, Hancke K, Winge P, Andresen K, Johnsen G, Bones AM. 2009. An integrated analysis of molecular acclimation to high light in the marine diatom *Phaeodactylum tricornutum*. *PLoS ONE* **4**: e7743.

Nymark M, Valle KC, Hancke K, Winge P, Andresen K, Johnsen G, Bones AM, Brembu T. 2013. Molecular and photosynthetic responses to prolonged darkness and subsequent acclimation to re-Illumination in the diatom *Phaeodactylum tricornutum*. *PLoS ONE* **8**: e58722.

Onarheim IH, Eldevik T, Smedsrud LH, Stroeve JC. 2018. Seasonal and regional manifestation of Arctic sea ice loss. *Journal of Climate* **31**: 4917–4932.

Oxborough K, Moore CM, Suggett DJ, Lawson T, Chan HG, Geider RJ. 2012. Direct estimation of functional PSII reaction center concentration and PSII electron flux on a volume basis: a new approach to the analysis of Fast Repetition Rate fluorometry (FRRf) data. *Limnology and Oceanography Methods* **10**: 142–154.

Pfannschmidt T. 2003. Chloroplast redox signals: how photosynthesis controls its own genes. *Trends in Plant Science* **8**: 33–41.

Pierrot DE, Lewis E, Wallace DWR. 2006. *MS excel program developed for CO_2 system calculations*. ORNL/OCDIAC-105a carbon dioxide information analysis centre. ORNL, TN, USA: US Department of Energy.

Pospíšil P, Yamamoto Y. 2017. Damage to photosystem II by lipid peroxidation products. *Biochimica et Biophysica Acta (BBA) – General Subjects* **1861**: 457–466.

Poulin M, Daugbjerg N, Gradinger R, Ilyash L, Ratkova T, von Quillfeldt C. 2011. The pan-Arctic biodiversity of marine pelagic and sea-ice unicellular eukaryotes: a first-attempt assessment. *Marine Biodiversity* **41**: 13–28.

Raven JA, Beardall J, Giordano M. 2014. Energy costs of carbon dioxide concentrating mechanisms in aquatic organisms. *Photosynthesis Research* **121**: 111–124.

Raven JA, Giordano M, Beardall J, Maberly SC. 2011. Algal and aquatic plant carbon concentrating mechanisms in relation to environmental change. *Photosynthesis Research* **109**: 281–296.

Richard D, Kefi K, Barbe U, Bausero P, Visioli F. 2008. Polyunsaturated fatty acids as antioxidants. *Pharmacological Research* **57**: 451–455.

Robinson MD, Oshlack A. 2010. A scaling normalization method for differential expression analysis of RNA-seq data. *Genome Biology* **11**: R25.

Rodriguez F, Chauton M, Johnsen G, Andresen K, Olsen L, Zapata M. 2006. Photoacclimation in phytoplankton: implications for biomass estimates, pigment functionality and chemotaxonomy. *Marine Biology* **148**: 963–971.

Rokitta SD, John U, Rost B. 2012. Ocean acidification affects redox-balance and ion-homeostasis in the life-cycle stages of *Emiliania huxleyi*. *PLoS ONE* **7**: e52212.

Rost B, Riebesell U, Sültemeyer D. 2006. Carbon acquisition of marine phytoplankton: effect of photoperiod length. *Limnology and Oceanography* **51**: 12–20.

Rost B, Zondervan I, Wolf-Gladrow D. 2008. Sensitivity of phytoplankton to future changes in ocean carbonate chemistry: current knowledge, contradictions and research directions. *Marine Ecology Progress Series* **373**: 227–237.

Screen JA, Simmonds I. 2010. The central role of diminishing sea ice in recent Arctic temperature amplification. *Nature* **464**: 1334–1337.

Shick JM, Dunlap WC. 2002. Mycosporine-like amino acids and related gadusols: biosynthesis, accumulation, and UV-protective functions in aquatic organisms. *Annual Review of Physiology* **64**: 223–262.

Stenbaek A, Jensen PE. 2010. Redox regulation of chlorophyll biosynthesis. *Phytochemistry* **71**: 853–859.

Stoll MHC, Bakker K, Nobbe GH, Haese RR. 2001. Continuous-flow analysis of dissolved inorganic carbon content in seawater. *Analytical Chemistry* **73**: 4111–4116.

Stroeve JC, Notz D. 2018. Changing state of Arctic sea ice across all seasons. *Environmental Research Letters* **13**: 103001.

Syvertsen EE. 1991. Ice algae in the Barents Sea: types of assemblages, origin, fate and role in the ice-edge phytoplankton bloom. *Polar Research* **10**: 277–288.

Szyszka B, Ivanov AG, Hüner NP. 2007. Psychrophily is associated with differential energy partitioning, photosystem stoichiometry and polypeptide phosphorylation in *Chlamydomonas raudensis*. *Biochimica et Biophysica Acta (BBA) – Bioenergetics* **1767**: 789–800.

Thompson PA, Harrison PJ, Parslow JS. 1991. Influence of irradiance on cell volume and carbon quota for ten species of marine phytoplankton. *Journal of Phycology* **27**: 351–360.

Tremblay J-É, Anderson LG, Matrai P, Coupel P, Bélanger S, Michel C, Reigstad M. 2015. Global and regional drivers of nutrient supply, primary production and CO_2 drawdown in the changing Arctic Ocean. *Progress in Oceanography* **139**: 171–196.

Trimborn S, Wolf-Gladrow D, Richter K-U, Rost B. 2009. The effect of pCO_2 on carbon acquisition and intracellular assimilation in four marine diatom species. *Journal of Experimental Marine Biology and Ecology* **376**: 26–36.

Tyystjärvi T, Mulo P, Mäenpää P, Aro E-M. 1996. D1 polypeptide degradation may regulate *psbA* gene expression at transcriptional and translational levels in *Synechocystis* sp. PCC 6803. *Photosynthesis Research* **47**: 111–120.

Van der Waal D, Brandenburg K, Keuskamp J, Trimborn S, Kranz S, Rokitta S, Rost B. 2019. Highest plasticity of carbon-concentrating mechanisms in earliest evolved phytoplankton: plasticity of carbon-concentrating mechanisms. *Evolutionary Plasticity of Carbon Concentrating Mechanisms in a Future Ocean* **4**: 37–43.

Wada N, Sakamoto T, Matsugo S. 2015. Mycosporine-like amino acids and their derivatives as natural antioxidants. *Antioxidants* **4**: 603.

Weeks WF, Ackley SF. 1986. The growth, structure, and properties of sea ice. In: Untersteiner N, ed. *The geophysics of sea ice*. Boston, MA: Springer US, 9–164.

Wolf KK, Hoppe CJ, Rost B. 2018. Resilience by diversity: large intraspecific differences in climate change responses of an Arctic diatom. *Limnology and Oceanography* **63**: 397–411.

Wu H, Roy S, Alami M, Green BR, Campbell DA. 2012. Photosystem II photoinactivation, repair, and protection in marine centric diatoms. *Plant Physiology* **160**: 464–476.

Wu Y, Campbell DA, Irwin AJ, Suggett DJ, Finkel ZV. 2014. Ocean acidification enhances the growth rate of larger diatoms. *Limnology and Oceanography* **59**: 1027–1034.

Yamamoto-Kawai M, McLaughlin FA, Carmack EC, Nishino S, Shimada K. 2009. Aragonite undersaturation in the arctic ocean: effects of ocean acidification and sea ice melt. *Science* **326**: 1098–1100.

Zhu S-H, Green BR. 2010. Photoprotection in the diatom *Thalassiosira pseudonana*: role of LI818-like proteins in response to high light stress. *Biochimica et Biophysica Acta (BBA) – Bioenergetics* **1797**: 1449–1457.

Supporting Information

Additional Supporting Information may be found online in the Supporting Information section at the end of the article.

Fig. S1 K-means clustering analysis of *Thalassiosira hyalina* and *Nitzschia frigida* based on Euclidean distances, using mean expression values, subtracting mean expression levels.

Fig. S2 Temporal changes of the turnover time of the electron transfer chain (τ_{ES}) in *Thalassiosira hyalina* (blue) and *Nitzschia frigida* (red) under low light (time 0) and after 1, 2, 3, 4, 5, 6, 12, 24, 48, 72, 96 and 120 h of HL exposure (380 μmol photons $m^{-1} s^{-1}$).

Methods S1 Detailed notes on materials and methods for differential gene expression analyses.

Notes S1 Benchmarking Universal Single-Copy Orthologs (BUSCO) and CD-hit analyses of *Thalassiosira hyalina* and *Nitzschia frigida.*

Table S1 Details on FRRf assay settings applied in this study.

Table S2 Statistical results from repeated measures (RM) ANOVA on the temporal development of photophysiological parameters and pigment quotas after low- to high light switch.

Table S3 Statistical results from two-way ANOVA with *post hoc* tests (Holm–Sidak) comparing growth rate, POC/PON, POC production and Chl*a* : POC between low light (LL), high light (HL), low pCO_2 (400 ppm) and high pCO_2 (1000 ppm) acclimated cells of *T. hyalina* and *N. frigida.*

Table S4 Statistical results from two-way ANOVA with *post hoc* tests (Holm–Sidak) comparing the effect of $pCO2$ levels on low light (LL) and high light (HL) acclimated cells.

Table S5 Experiment metadata, including sample list as well as descriptive statistics regarding sequencing and post-processing.

Table S6 List of *de novo* assembled transcripts obtained for the two species.

Table S7 Excel sheet containing expression data, results of statistical significance tests, BLAST annotations as well as functional classification of the reduced set of genes of interest.

Table S8 BLASTX annotation table.

Please note: Wiley Blackwell are not responsible for the content or functionality of any Supporting Information supplied by the authors. Any queries (other than missing material) should be directed to the *New Phytologist* Central Office.